The effect of hydroelasticity on ship slamming

O. M. Faltinsen

Email alerting service	Receive free email alerts when new articles cite this article - sign up in the box at the top right-hand corner of the article or click **here**

The effect of hydroelasticity on ship slamming

By O. M. Faltinsen

*Department of Marine Hydrodynamics, Norwegian University of
Science and Technology, N-7034 Trondheim, Norway*

Wetdeck slamming is studied theoretically by a hydroelastic beam model. The problem is simplified by introducing an initial structural inertia phase and a subsequent free vibration phase. Forward speed effects are included. The theoretical model is validated by comparing with drop tests of elastic plates on waves. The stresses in the plates have a linear dependence on the impact speed and are neither sensitive to the radius of curvature of the waves nor where the waves initially hit. Hydroelasticity is important. The maximum impact pressures can be extremely high and have a stochastic nature even under deterministic environmental conditions, but they are not important for maximum bending stresses.

1. Introduction

Impact between the water and a ship, i.e. slamming, can cause important local and global loads on a vessel. Slamming on ship hulls is often categorized as bottom slamming and bow flare slamming. When a bow flare section of a ship enters the water, the local loads around the flare are not influenced by hydroelasticity. However, hydroelasticity is important in a global analysis. By considering the ship hull as an elastic beam, the integrated water-entry force on a bow flare section causes transient hydroelastic response (whipping) of the beam.

When the local loads become very high, as during wetdeck slamming, hydroelasticity is also important for the local loads. By wetdeck is meant the structural part connecting the two side hulls of a catamaran. Very high pressures can be measured during wetdeck slamming. The idealized theory presented in the main text models the part of the wetdeck between two transverse stiffeners by an Euler beam with length L corresponding to the distance between the transverse stiffeners. This means that the beam deflections are dominated by those of the longitudinal stiffeners. The transverse stiffeners can be assumed to be much stiffer than the longitudinal stiffeners (Kvålsvold 1994; Kvålsvold & Faltinsen 1995). Either aluminium or steel is implicitly assumed.

An asymptotic hydroelastic theory is presented for a nearly horizontal beam that hits the water close to a wave crest. The beam can both have a forward speed U and a drop velocity V. The ratio V/U is either small or large in the analysis. The effect of the forward speed is incorporated in the body boundary conditions and the free surface conditions. Solutions for steady state oscillations of a hydrofoil in infinite fluid are used. It is shown theoretically that the forward speed effects due to the free surface conditions are not significant for realistic forward speeds and structural dimensions. The problem is divided into two time scales. A large hydrodynamic force

TEX Paper

causes a large acceleration of a small structural mass in the first time scale. The time scale is short relative to the second time scale, which is the highest wet natural period of the beam. The behaviour in the second time scale is a free elastic vibration with initial conditions obtained from the first time scale.

A motivation for developing the asymptotic theory is that high numerical accuracy is needed to describe all the details of wetdeck slamming during the initial phase (Kvålsvold & Faltinsen 1995). Extensive use of analytical expressions is necessary. This is possible when a two-dimensional hydrodynamic model and structural beam model are used. If the flow is three-dimensional and a more complete structural modelling of the wetdeck is used, the procedure has to be based on a more direct numerical method. Numerical difficulties will arise in the initial phase when using a direct numerical procedure.

The asymptotic theory shows that the maximum bending stresses are proportional to an effective drop velocity and are not sensitive to the curvature of the waves or where the waves hit the beam. This has been experimentally confirmed by drop tests of horizontal elastic plates on waves of different steepnesses (Kvålsvold *et al.* 1995; Aarsnes 1994).

2. Theory

The structure is represented by an Euler beam model. The analysis by Kvålsvold & Faltinsen (1995) showed that the effect of shear deformation on the hydroelastic response was not essential. The structure in the following application is a beam of constant thickness and finite breadth, but a similar structural formulation was used for the wetdeck between two transverse stiffeners by Kvålsvold & Faltinsen (1995). The beam equation of motion is written as

$$M_{\mathrm{B}}\frac{\partial^2 w}{\partial t^2} + EI\frac{\partial^4 w}{\partial x^4} = p(x, w, t). \tag{2.1}$$

Here M_{B} is the structural mass per unit length and breadth of the beam, $w(x,t)$ is the elastic beam deflection, t is the time variable and x is a longitudinal coordinate along the length L of the beam. EI is the bending stiffness, so that E is the Youngs modulus and I is the area moment of inertia of the beam cross-section divided by the breadth of the beam. Further p is the pressure that is a function of the beam deflections. M_{B} and EI are assumed constant. Rigid body accelerations are neglected since it will be small relative to the acceleration term in equation (2.1). Boundary and initial conditions are also needed. The solution is expressed in terms of dry normal modes ψ_i, i.e.

$$w(x,t) = \sum_{i=1}^{\infty} a_i(t)\psi_i(x). \tag{2.2}$$

The eigenfunctions satisfy equation (2.1) with $p = 0$ and the boundary conditions $\psi_i = 0$ and

$$\frac{k_\theta}{EI}\frac{\partial \psi_i}{\partial x} \pm \frac{\partial^2 \psi_i}{\partial x^2} = 0 \tag{2.3}$$

at the beam ends $x = \pm(\frac{1}{2}L)$. Here k_θ is a spring stiffness that is related to a restoring moment $-k_\theta\theta_{\mathrm{be}}$ at the beam ends. θ_{be} is the rotation angle at a beam end. The symmetric eigenfunctions are

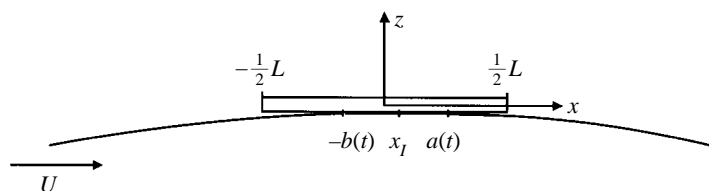$$\psi_i = \cos p_i x + D_i \cosh p_i x, \tag{2.4}$$

Figure 1. Coordinate system fixed to the beam. U = forward speed. $x = x_I$ initial point of impact without air cushion.

where p_i are determined as the solutions of

$$K_\theta P_i(\cos P_i \sinh P_i + \cosh P_i \sin P_i) + 2P_i^2 \cos P_i \cosh P_i = 0, \qquad (2.5)$$

where P_i and K_θ are defined as $P_i = 0.5p_iL$ and $K_\theta = 0.5k_\theta L/EI$. Further $D_i = -\cos P_i/\cosh P_i$.

The hydrodynamic pressure is found by solving a boundary value problem in an incompressible fluid. Kvålsvold & Faltinsen (1995) showed that compressibility effects were not important for the maximum stresses. The flow is irrotational and described by a velocity potential. The fluid accelerations are assumed to be much larger than the acceleration due to gravity.

Let ϕ be the perturbation velocity potential in the fluid due to the impact. The velocity potential satisfies a two-dimensional Laplace equation in the fluid. A relative frame of coordinate system fixed to the beam is used so that the forward speed U of the beam appears as an incident flow along the positive horizontal x-axis (see figure 1). If the beam has a small rotation α around the y-axis, the beam is projected on the x-axis in the analysis.

The body boundary condition can be approximated by

$$\frac{\partial \phi}{\partial z} = -V - U\alpha - u_z + \frac{\partial w}{\partial t} + U\frac{\partial w}{\partial x}, \quad \text{on } z = 0. \qquad (2.6)$$

Here V is the vertical rigid body drop velocity of the beam. It is positive downwards. α is a rigid body rotation about the y-axis. Positive α means that $x = \frac{1}{2}L$ is downwards relative to $\alpha = 0$. Furthermore u_z is the vertical velocity of the incident waves at the impact position. An effective rigid body drop velocity V_e can be defined from equation (2.6), i.e.

$$V_e = V + U\alpha + u_z. \qquad (2.7)$$

Because the structure hits the water close to a wave crest, u_z will in reality be zero or small relative to V. A Kutta condition is needed when U is different from zero. The free surface boundary conditions will be introduced later. The boundary value problem will be solved by matched asymptotic expansions in time.

3. Structural inertia phase

Two flow pictures are possible in the initial phase. Either the beam touches the water initially in one point or the water can be raised close to the ends of the beam and a compressible air cushion created between the beam and the free surface. This will depend on the curvature of the waves at the impact position. The air cushion effect is less probable if the beam is part of a long wetdeck. It is first assumed that no air pocket is entrapped. This is the case Kvålsvold & Faltinsen (1995) studied.

The waves hit initially at $x = x_I$. $\psi_i(x)$ is approximated by $\psi_i(x_I)$ over the initially wetted part.

The time rate of change is much larger than the spatial rate of change. Equation (2.6) is approximated as

$$\frac{\partial \phi}{\partial z} = \sum \dot{a}_i(t)\psi_i(x_I) - V_e, \quad \text{on} \ -b(t) \leqslant x \leqslant a(t), \quad \text{and} \quad z = 0. \tag{3.1}$$

Further

$$\phi = 0 \text{ on } z = 0, \quad \text{for } x < -b(t), \quad \text{and} \quad x > a(t). \tag{3.2}$$

Dot stands for time derivative. The wetted surface between $x = -b(t)$ and $a(t)$ can be found by Wagner's procedure (1932). The wetting due to spray is then neglected. When $U = 0$, the solution has similarities with Wagner's solution for water entry of a cylinder with radius R. R means the radius of curvature of the incident waves at the position of initial impact. The speed $dc(t)/dt$ of the intersection points between the water and the beam will initially be infinite. This implies that the compressibility effect of the water is significant up to the time when $dc(t)/dt$ is the order of magnitude of the speed of sound in water. This time scale is small relative to the time scale of the structural inertia phase. The maximum pressures occur when the compressibility of the water matters, but this is not important for the resulting maximum bending stresses in the beam; the pressures are too concentrated in time and space. The solution is formally written

$$\phi = \phi^N(x)\left(\sum \dot{a}_i\psi_i(x_I) - V_e\right). \tag{3.3}$$

The following relation applies

$$\int_{S_w} \phi^N \, dx = A_{33}. \tag{3.4}$$

Here S_w is the wetted length and A_{33} is the added mass in heave with free surface condition $\phi = 0$.

The bending stiffness term in the beam equation can initially be neglected, i.e.

$$M_B \frac{\partial^2 w}{\partial t^2} = \begin{cases} -\rho\dfrac{\partial \phi}{\partial t}, & \text{on} \ -b(t) < x < a(t), \\ 0, & \text{on} \ -\frac{1}{2}L < x < -b(t), \, a(t) < x < \frac{1}{2}L. \end{cases} \tag{3.5}$$

By integrating this equation in time with initial conditions $\phi = 0$ and $w = 0$, multiplying the resulting equation by $\psi_j(x)$ and integrating over the length of the beam, it follows that

$$\sum_{i=1}^{\infty} \dot{a}_i \int_{-(L/2)}^{(L/2)} M_B \psi_i \psi_j \, dx = \rho\psi_j(x_I)\left(\sum \dot{a}_i\psi_i(x_I) - V_e\right)A_{33}. \tag{3.6}$$

Since the wetted length is small relative to L, $\psi_i(x_I)$ in equation (3.3) can be approximated by $\psi_i(x)$ for $-b(t) < x < a(t)$. The same is true in the brackets of the right-hand side of equation (3.6). An outer expansion is obtained by letting $t \to \infty$ relative to the initial time scale. Since $\dot{a}_i$ has to be finite, the left-hand side of equation (3.6) is finite. Since A_{33} increases with time on the right-hand side, the only

possibility for the right-hand side to be finite is that

$$\left(V_{\mathrm{e}} - \sum_{i=1}^{\infty} \dot{a}_i \psi_i(x) \right) \to 0, \tag{3.7}$$

as $t \to \infty$. Equation (3.7) applies on the wetted length. Since the wetted length goes to infinity when $t \to \infty$ in the initial time scale, equation (3.7) applies for all x-values on the beam when $t \to \infty$. Since t is small in the structural inertia phase, integrating equation (3.5) twice in time implies that w is an order of magnitude smaller than $\partial w / \partial t$. A first approximation is $w = 0$.

The time scale T_{s} in the structural inertia phase follows by using equation (3.5), scaling the wetted length by $(V_{\mathrm{e}} T_{\mathrm{s}} R)^{1/2}$ and $\partial w / \partial t$ by V_{e}. The scaling of the wetted length follows from Wagner's solution. It follows that

$$T_{\mathrm{s}} = \frac{M_{\mathrm{B}}^2}{\rho^2 V_{\mathrm{e}} R}. \tag{3.8}$$

The time scale $T_N = (\rho L^5 / EI)^{1/2}$ of the free vibration phase is derived by Kvålsvold & Faltinsen (1995). T_{s} must be less than T_N. This is satisfied for dimensions relevant for wetdeck slamming. It is also required that the length scale of the wetted length is much less than L. This means that $M_{\mathrm{B}}/\rho L$ is small, which is true in practice.

If the radius of curvature R of the wave crest is large and there are no forward speed effects, an air cushion is created between the beam and the free surface in an initial phase. The air cushion pressure $p_{\mathrm{ac}}(t)$ is assumed space independent and can be related to the air cushion mass density $\rho_{\mathrm{ac}}(t)$ by an isentropic air compression relationship. This means that $p_{\mathrm{ac}}(t)$ is proportional to $\rho_{\mathrm{ac}}^{\gamma}$, where γ is the specific heat ratio of air. The continuity equation for the air cushion is written as $\mathrm{d}(\rho_{\mathrm{ac}} \Omega)/\mathrm{d}t = 0$. Ω is the two-dimensional air cushion volume, where $\Omega \approx h(t)L$ and

$$\mathrm{d}\Omega / \mathrm{d}t \approx \int_{-(L/2)}^{(L/2)} \left(\frac{\partial w}{\partial t} - V \right) \mathrm{d}x; \tag{3.9}$$

$h(t)$ is an average thickness of the air cushion. Equation (3.9) is based on the fact that the free surface velocity $\partial \zeta / \partial t$ is small relative to $\partial w / \partial t$. It can be shown that the ratio of $\partial \zeta / \partial t$ to $\partial w / \partial t$ is $O(M_{\mathrm{B}}/\rho L)$. This follows by analysing the water flow caused by $p_{\mathrm{ac}}(t)$ (Verhagen 1967) and using that

$$M_{\mathrm{B}} \frac{\partial^2 w}{\partial t^2} = p_{\mathrm{ac}} - p_{\mathrm{a}}, \tag{3.10}$$

where p_{a} is atmospheric pressure.

The continuity equation can be written as

$$M_{\mathrm{B}} \frac{\partial^3 w}{\partial t^3} h(t) L = \gamma p_{\mathrm{ac}}(t) \int_{-(L/2)}^{(L/2)} \left(V - \frac{\partial w}{\partial t} \right) \mathrm{d}x. \tag{3.11}$$

This follows by first writing $\mathrm{d}\rho_{\mathrm{ac}}/\mathrm{d}t$ and ρ_{ac} in terms of $\mathrm{d}p_{\mathrm{ac}}/\mathrm{d}t$ and p_{ac} and then use equation (3.10) to express $\mathrm{d}p_{\mathrm{ac}}/\mathrm{d}t$. When the air pocket collapses, i.e. $h(t) \to 0$, $p_{\mathrm{ac}}(t)$ approaches a non-zero value. This implies from equation (3.11) that

$$\int_{-(L/2)}^{(L/2)} \left(V - \frac{\partial w}{\partial t} \right) \mathrm{d}x \to 0 \tag{3.12}$$

as $h(t) \to 0$. The time scale T_{ac} of the air cushion process is found from equation (3.11). By using measured data by Miyamoto & Tanizawa (1985) for the thickness of the air layer and the air cushion pressure for a rigid plate it follows that T_{ac} is small relative to the time scale of the free vibration scale. It follows then that the behaviour of the beam at the end of the time phase is similar to the first case.

4. Free vibration phase

The second time phase has a time scale of the highest natural wetted period T_N. The problem can be thought of as an initial value problem where at $t = 0$

$$\sum \dot{a}_i(0)\psi_i(x) = V_{\mathrm{e}} \tag{4.1}$$

and the deflection $w = 0$. This is a consequence of matching with the initial phase solution.

It is only necessary to consider the lowest mode shape corresponding to the highest natural period. One reason is that the amplitudes of the higher modes have initially lower amplitudes than the lowest mode. This is a consequence of the initial conditions. In addition the damping is relatively large for the higher modes. The higher modes will nearly disappear on the scale of the period of the lowest mode. If the modes higher than the lowest mode should be important, there is a contradiction. The natural periods associated with the higher modes are not larger than the time scale of the structural inertia phase.

The structural vibrations are obtained from equation (2.1). The hydrodynamic pressure causes an added mass and damping effect. This will be derived when the forward speed U is large relative to the vertical rigid body drop velocity V. It turns out that the solution for large V/U-values is a special case of this solution.

The generalized added mass and damping are found by forcing the beam to oscillate harmonically with a vertical deflection

$$w(x) = \overline{Z}_1 \psi_1(x)\mathrm{e}^{\mathrm{i}\omega t}, \quad \text{where } \mathrm{i}^2 = -1. \tag{4.2}$$

It is understood that the real part has physical meaning. Steady state conditions are assumed. The boundary value problem for the velocity potential ϕ is

$$\frac{\partial \phi}{\partial z} = \left[\mathrm{i}\omega\overline{w}(x) + U\frac{\partial\overline{w}(x)}{\partial x}\right]\mathrm{e}^{\mathrm{i}\omega t} \equiv \overline{w}_{\mathrm{a}}(x)\mathrm{e}^{\mathrm{i}\omega t}, \quad \text{on } z = 0^-, \ |x| \leqslant (\tfrac{1}{2}L), \tag{4.3}$$

$$\phi = 0 \quad \text{on } z = 0, \quad \text{for } x < -(\tfrac{1}{2}L), \tag{4.4}$$

$$\mathrm{i}\omega\phi + U\frac{\partial\phi}{\partial x} = 0, \quad \text{on } z = 0, \quad \text{for } x > (\tfrac{1}{2}L). \tag{4.5}$$

There is a Kutta condition requiring finite velocities and continuity in the pressure at the trailing edge $x = (\tfrac{1}{2}L)$.

The boundary value problem so defined is similar to the linear unsteady hydrofoil problem in infinite fluid. This is discussed by Ulstein & Faltinsen (1994), who used a numerical time domain solution to study the water impact of a flexible aft seal bag of an SES at high forward speed.

The pressure distribution on the beam is presented by Bisplinghoff *et al.* (1955). The solution is for a harmonically oscillating foil in infinite fluid. The pressure $\overline{p}_{\mathrm{L}}\mathrm{e}^{\mathrm{i}\omega t}$

on the lower side of the beam can be written as

$$\frac{\overline{p}_{\mathrm{L}}(x^*)}{\rho U} = \frac{1}{\pi}\left[1 - C(k^*)\right]\sqrt{\frac{(1-x^*)}{(1+x^*)}}\int_{-1}^{1}\sqrt{\frac{(1+\xi^*)}{(1-\xi^*)}}\overline{w}_{\mathrm{a}}(\xi^*)\,\mathrm{d}\xi^*$$

$$+\frac{1}{\pi}PV\int_{-1}^{1}\left[\sqrt{\frac{(1-x^*)}{(1+x^*)}}\sqrt{\frac{(1+\xi^*)}{(1-\xi^*)}}\frac{1}{x^*-\xi^*} - \mathrm{i}k^*\varLambda_1(x^*,\xi^*)\right]\overline{w}_{\mathrm{a}}(\xi^*)\,\mathrm{d}\xi^*, \quad (4.6)$$

where the coordinates $x^* = x/(\frac{1}{2}L)$ and $\xi^* = \xi/(\frac{1}{2}L)$. PV means principal value integral. Further

$$\varLambda_1 = \frac{1}{2}\ln\left[\frac{1 - x^*\xi^* + \sqrt{1-\xi^{*2}}\sqrt{1-x^{*2}}}{1 - x^*\xi^* - \sqrt{1-\xi^{*2}}\sqrt{1-x^{*2}}}\right], \quad (4.7)$$

$$C(k^*) = \frac{H_1^{(2)}(k^*)}{H_1^{(2)}(k^*) + \mathrm{i}H_0^{(2)}(k^*)}, \quad (4.8)$$

$$k^* = \omega(\tfrac{1}{2}L)/U, \quad (4.9)$$

$$H_n^{(2)} = J_n - \mathrm{i}Y_n, \quad (4.10)$$

where J_n and Y_n are Bessel functions of the first and second kind and $H_n^{(2)}$ is a Hankel function (Watson 1958). $C(k^*)$ is the Theodorsen function. $\overline{w}_{\mathrm{a}}$ in equation (4.6) can be expressed in terms of ψ_1 and written as

$$\overline{w}_{\mathrm{a}}(x) = \mathrm{i}\omega\overline{Z}_1(\cos(p_1 x) + D_1\cosh(p_1 x)) + U\overline{Z}_1 p_1(-\sin(p_1 x) + D_1\sinh(p_1 x)); \quad (4.11)$$

$\overline{w}_{\mathrm{a}}(x)$ is rewritten as a Fourier series where

$$\overline{w}_{\mathrm{a}}(x) = \sum_{n=0}^{\infty} A_n\cos n\theta \quad (4.12)$$

and

$$x = (\tfrac{1}{2}L)\cos\theta, \quad 0 \leqslant \theta \leqslant \pi. \quad (4.13)$$

It follows that

$$A_0 = \mathrm{i}\omega\overline{Z}_1(J_0(P_1) + D_1 I_0(P_1)), \quad (4.14)$$

$$A_{2n} = \mathrm{i}\omega\overline{Z}_1 2((-1)^n J_{2n}(P_1) + D_1 I_{2n}(P_1)), \quad (4.15)$$

$$A_{2n+1} = U Z_1 p_1 2(-(-1)^n J_{2n+1}(P_1) + D_1 I_{2n+1}(P_1)), \quad (4.16)$$

where I_n is the modified Bessel function (Watson 1958). By using equation (4.12) in equation (4.6) it follows after some calculations and use of integral relations that

$$\frac{\overline{p}_{\mathrm{L}}(x^*)}{\rho U} = [1 - C(k^*)]\sqrt{\frac{(1-x^*)}{(1+x^*)}}(A_0 + \tfrac{1}{2}A_1)$$

$$-\frac{1}{2}\sqrt{\frac{(1-x^*)}{(1+x^*)}}\sum_{n=0}^{\infty}A_n\left[2\frac{\sin n\chi}{\sin\chi} + \frac{\sin(n+1)\chi}{\sin\chi} + \frac{\sin|n-1|\chi}{\sin\chi}\right]$$

$$-\mathrm{i}k^*\frac{1}{2}\sum_{n=0}^{\infty}A_n\left[\frac{1}{n+1}\sin(n+1)\chi + \frac{L_n}{|1-n|}\sin(1-n)\chi\right], \quad (4.17)$$

where $L_n = 0$ when $n = 1$ and $L_n = 1$ for $n \neq 1$. Further

$$x^* = \cos \chi, \quad 0 \leqslant \chi \leqslant \pi. \tag{4.18}$$

Generalized added mass and damping is introduced by multiplying equation (4.17) with the mode shape and integrating over the length of the beam. This leads to the generalized force

$$F_3^G = (\tfrac{1}{2}L) \int_{-1}^{1} \overline{p}_L(x^*)(\cos(P_1 x^*) + D_1 \cosh(P_1 x^*))\, \mathrm{d}x^*. \tag{4.19}$$

The generalized added mass A_{11} and damping B_{11} are defined by

$$F_3^G \equiv -A_{11}(-\omega^2 \overline{Z}_1) - B_{11}\mathrm{i}\omega \overline{Z}_1. \tag{4.20}$$

It requires some calculations and use of integral relations to derive the following formulas for A_{11} and B_{11}. ψ_1 is written as a Fourier series $\sum W_k \cos k\chi$, where

$$W_0 = (J_0(P_1) + D_1 I_0(P_1)), \tag{4.21}$$

$$W_{2k} = 2((-1)^k J_{2k}(P_1) + D_1 I_{2k}(P_1)). \tag{4.22}$$

The added mass for $U = 0$ is denoted by A_{11}^0 and is similar to that which Kvålsvold (1994) derived by a different approach. It follows that

$$A_{11}^0 = \rho(\tfrac{1}{2}L)^2 \tfrac{1}{4}\pi(J_0(P_1) + D_1 I_0(P_1))\Big\{ 2(J_0(P_1) + J_2(P_1)) + 2D_1(I_0(P_1) - I_2(P_1)) \Big\}$$

$$+ \rho(\tfrac{1}{2}L)^2 \tfrac{1}{2}\pi \sum_{k=1}^{\infty} ((-1)^k J_{2k}(P_1) + D_1 I_{2k}(P_1))$$

$$\times \Big\{ \frac{1}{(2k+1)}[(-1)^k(J_{2k}(P_1) + J_{2k+2}(P_1)) + D_1(I_{2k}(P_1) - I_{2k+2}(P_1))]$$

$$+ \frac{1}{|1-2k|}[(-1)^k(J_{2k}(P_1) + J_{2k-2}(P_1)) + D_1(I_{2k}(P_1) - I_{2k-2}(P_1))] \Big\}. \tag{4.23}$$

The complete added mass can be written as

$$A_{11} = A_{11}^0 + \rho(\tfrac{1}{2}L)^2 \frac{\pi}{k^*} \mathrm{Im}[C(k^*)](J_0(P_1) + D_1 I_0(P_1))^2$$

$$+ \rho(\tfrac{1}{2}L)^2 \frac{\pi}{k^{*2}} P_1(1 - \mathrm{Re}[C(k^*)])(J_0(P_1) + D_1 I_0(P_1))(-J_1(P_1) + D_1 I_1(P_1))$$

$$- \rho(\tfrac{1}{2}L)^2 \frac{\pi}{k^{*2}} \tfrac{1}{2}P_1 \sum_{m=0}^{\infty} \Big\{ (-(1)^m J_{2m+1}(P_1) + D_1 I_{2m+1}(P_1))$$

$$\times \Big[\sum_{k=0}^{\infty} W_{2k}(\tfrac{1}{2} + \mathrm{sgn}(2m+1-2k) - \tfrac{1}{2}\mathrm{sgn}(2m+3-2k)$$

$$- \tfrac{1}{2}\mathrm{sgn}(2m-2k-1) - \tfrac{1}{2}\mathrm{sgn}(2m+2k-1)) \Big] \Big\}, \tag{4.24}$$

where Re and Im mean, respectively, real and imaginary part and sgn means the sign of. The damping can be written as

$$B_{11} = \rho U(\tfrac{1}{2}L)\pi \, \mathrm{Re}[C(k^*)](J_0(P_1) + D_1 I_0(P_1))^2$$

$$+ \rho U(\tfrac{1}{2}L)\pi \frac{P_1}{k^*} \mathrm{Im}[C(k^*)](J_0(P_1) + D_1 I_0(P_1)(-J_1(P_1) + D_1 I_1(P_1)). \tag{4.25}$$
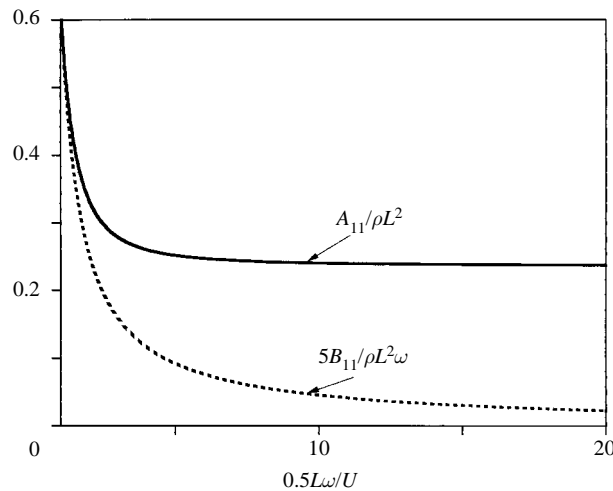
Figure 2. Generalized added mass A_{11} and damping B_{11} as a function of reduced frequency $0.5\omega L/U$. $M_\mathrm{B}/\rho L = 0.124$. $k_\theta L/EI = 5.7$.

Equations (4.24) and (4.25) have been independently controlled by integrating equation (4.19) numerically. Since the behaviour of A_{11} and B_{11} as a function of $k^* = \frac{1}{2}\omega L/U$ is very similar for different values of mass and spring stiffnesses, only one case of non-dimensionalized added mass and damping coefficients is presented (see figure 2). The asymptotic values of $B_{11}/(\rho L^2\omega)$ and $A_{11}/(\rho L^2)$ are respectively zero and $A_{11}^0/(\rho L^2)$ when $k* \to \infty$.

The equation of structural vibrations is obtained by using the lowest mode, multiplying equation (2.1) with $\psi_1(x)$ and integrating from $x = -(\frac{1}{2}L)$–$(\frac{1}{2}L)$. It follows that

$$\left[M_{11} + A_{11}\right]\ddot{a}_1(t) + B_{11}\dot{a}_1(t) + \left[p_1^4 EI \int_{-(\frac{1}{2}L)}^{(\frac{1}{2}L)} \psi_1^2\,\mathrm{d}x\right]a_1(t) = 0, \tag{4.26}$$

where

$$\int_{-(L/2)}^{(L/2)} \psi_1^2\,\mathrm{d}x = \frac{1}{2p_1}(\sin 2P_1 + 2P_1) + 2\frac{D_1}{p_1}(\sinh P_1 \cos P_1 + \cosh P_1 \sin P_1)$$

$$+\frac{D_1^2}{2p_1}(2P_1 + \sinh 2P_1). \tag{4.27}$$

The wet natural undamped circular frequency ω_w follows from equation (4.26) as

$$\omega_\mathrm{w}\sqrt{\frac{\rho L^5}{EI}} = 4P_1^2 \sqrt{\int_{-(L/2)}^{(L/2)} \psi_1^2(x)\,\mathrm{d}x/L \Big/ \left(\frac{M_\mathrm{B}}{\rho L} \int_{-(L/2)}^{(L/2)} \psi_1^2(x)\,\mathrm{d}x/L + A_{11}/\rho L^2\right)}. \tag{4.28}$$

The undamped solution for w can be written as

$$w = \bar{a}_1\psi_1 \sin\omega_\mathrm{w}t. \tag{4.29}$$

This automatically satisfies the initial condition $w = 0$; a_1 is determined by the

Table 1. *Generalized added mass A_{11}, wet natural frequencies ω_{w}, and bending stresses σ_{b} as a function of mode shapes. $\sigma_{\mathrm{b}} = \sigma_{\mathrm{ba}} \sin \omega_{\mathrm{w}} t$ (zero forward speed)*

| | | | | $\dfrac{\sigma_{\mathrm{ba}}}{(z_{\mathrm{a}}/L)V_{\mathrm{e}}} \sqrt{I/(\rho L^3 E)}$ | | | |
| | | | | $x/L =$ | | | |
$M_{\mathrm{B}}/(\rho L)$	$k_\theta L$	A_{11}	$\omega_{\mathrm{w}} \sqrt{\rho L^5/(EI)}$	0.0	0.2	0.4	0.5
0.02	0.0	0.21	14.76	0.85	0.69	0.26	0.0
	0.5	0.23	17.3	0.78	0.59	0.09	-0.21
	1.75	0.24	21.27	0.72	0.48	-0.12	-0.48
	2.85	0.24	23.43	0.70	0.44	-0.22	-0.61
	5.0	0.23	26.04	0.68	0.40	-0.32	-0.75
0.124	0.0	0.21	13.29	0.95	0.76	0.29	0.0
	0.5	0.23	15.57	0.87	0.66	0.10	-0.23
	1.75	0.24	19.15	0.80	0.54	-0.13	-0.53
	2.85	0.24	21.08	0.77	0.49	-0.24	-0.68
	5.0	0.23	23.42	0.76	0.44	-0.36	-0.83
	20.0	0.22	27.97	0.74	0.37	-0.55	-1.09
	10^4	0.21	30.68	0.74	0.33	-0.65	-1.21

initial conditions for the velocity, i.e.

$$\bar{a}_1 \omega_{\mathrm{w}} \int_{-(L/2)}^{(L/2)} \psi_1^2 \, \mathrm{d}x = V_{\mathrm{e}} \int_{-(L/2)}^{(L/2)} \psi_1 \, \mathrm{d}x = V_{\mathrm{e}} \left(\frac{1}{p_1} \sin P_1 + \frac{D_1}{p_1} \sinh P_1 \right). \qquad (4.30)$$

The resulting non-dimensionalized bending stress σ_{b} can be written as

$$\frac{\sigma_{\mathrm{b}}}{(z_{\mathrm{a}}/L)V_{\mathrm{e}}} \sqrt{\frac{I}{\rho E L^3}} = \frac{4P_1^2}{\omega_{\mathrm{w}} \sqrt{\rho L^5/(EI)}} \left(\int_{-(L/2)}^{(L/2)} \psi_1(x) \, \mathrm{d}x \bigg/ \int_{-(L/2)}^{(L/2)} \psi_1^2(x) \, \mathrm{d}x \right)$$

$$\times \left(\cos(p_1 x) + \frac{\cos P_1}{\cosh P_1} \cosh(p_1 x) \right) \sin \omega_{\mathrm{w}} t. \qquad (4.31)$$

Here z_{a} is the distance from the neutral axis to the point where the stresses are calculated.

Table 1 shows calculations for $U = 0$. $M_{\mathrm{B}}/\rho L$ is not an important parameter. The table shows that the stresses and natural frequencies are more influenced by the spring constant k_θ.

The effect of forward speed on slamming response is illustrated in figure 3 when $M_{\mathrm{B}}/\rho L = 0.124$ and $\frac{1}{2} k_\theta L/EI = 2.85$. Non-dimensionalized values for ω_{w} as a function of $k^* = 0.5 \omega_{\mathrm{w}} L/U$ are presented. An iteration procedure is needed to find corresponding values of ω_{w} and U. The non-dimensionalized undamped bending stress amplitude σ_{ba} at $x = 0$ and the ratio between the damping and the critical damping are also shown in figure 3.

Figure 3 shows that the influence of forward speed on non-dimensionalized bending stress starts to be pronounced for k^* less than approximately three. If realistic values
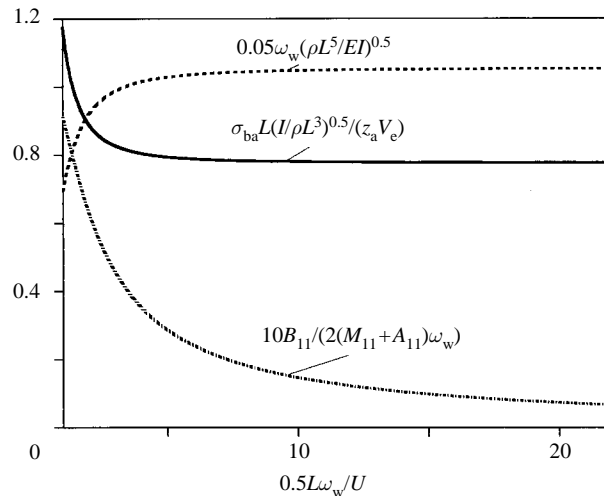
Figure 3. Influence of forward speed on slamming response of a nearly horizontal plate as a function of reduced frequency $0.5\omega_{\mathrm{w}}L/U$: ω_{w}, wet natural frequency; σ_{ba}, maximum undamped bending stress in the middle of the beam; B_{11}, generalized damping; $2(M_{11} + A_{11})\omega_{\mathrm{w}}$, critical damping; $M_{\mathrm{B}}/\rho L = 0.124$, $k_\theta L/EI = 5.7$.

for wetdeck slamming are used for ω_{w} and U, k^* is not expected to be that low. However, since the bending stress σ_{b} is proportional to V_{e}, U will influence σ_{b}.

Only small and large values of V/U have been studied. Even if the formulae for small values of V/U contain the results for $U = 0$, it is no proof that the formulation is valid for finite values of V/U.

5. Experimental validation

Aarsnes (1994) and Kvålsvold *et al.* (1995) presented experimental results from drop tests with a horizontal elastic plate on regular propagating waves of different steepnesses. A newly developed free-falling rig was used in the towing tank of the Marine Technology Centre in Trondheim.

The shape of the plate is shown in figure 4. The material is steel. The total drop section was divided into three parts, one measuring section with a dummy section on each side as shown in the figure. The measuring section was connected to the rig using two force transducers. The total weight of the measuring section includes the weight of the test plate in addition to the support system of the plate, i.e. it represents the total weight of the section connected underneath the vertical force transducers (see figure 4). This weight is 14 kg. The thickness of the elastic plate is 8 mm. The material density is 7850 kg m^{-3} and the E modulus is 210×10^9 N m^{-2}. It follows that I is 4.266×10^{-8} m^4 m^{-1} and $M_{\mathrm{B}}/\rho L = 0.124$. The thickness and the stiffness of the dummy section plates were the same as for the measuring section. The total weight of the drop rig was 500 kg.

The instrumentation in the test consists of pressure cells, vertical force transducers connected to the measuring section, wetted surface measurements using wave gauges tape, accelerometers to determine the accelerations in the rig and the measuring plate, drop velocity measurements, strain measurements using strain gauges in four different positions on the plate, vertical deflection of the plate using displacement transducer and wave staffs. The diameter of each pressure cell was 4 mm. The tests
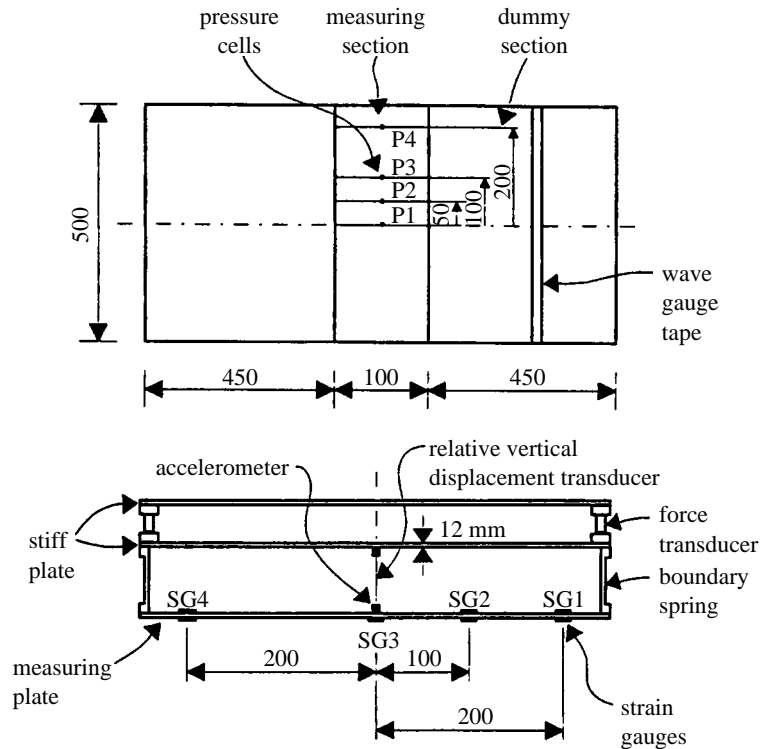
Figure 4. Details of the elastic test plate (Aarsnes 1994).

were carried out for drop speeds ranging from 2.2 m s^{-1} to 6.2 m s^{-1}. The radius R of the wave crest for the different waves varied from 1.5–10 m. For incident regular waves of small amplitudes ζ_a, R is expressed as $(k^2\zeta_a)^{-1}$ where k is the wave number. In addition, drop against calm water (i.e. $R = \infty$) was included. The wave crest hits the centre of the plate in most cases. However, for some test conditions, the position where the wave crest hits the plate was systematically varied. The forward speed is zero.

Before the drop tests, the end connecting moment of the plate was determined. The associated spring stiffness $k_\theta = 5.7EI/L$ was obtained. The experimental results showed that the maximum measured strains were proportional to the drop velocity and independent of the wave crest radius R as long as R had realistic values for ship applications. Typical values are $L/R = 0.005$–0.02. This is based on the premise that wetdeck slamming is mainly a problem for wave lengths l corresponding to the natural period of the pitch motions, which occurs for $l = 1$–1.5 times the ship length and by assuming a ship length of 80 m, a wave height of 5 m and $L = 1$ m. The maximum strains showed very small sensitivity to where the wave crest initially hit the plate as long as the wave crest hit between the two beam ends. All these findings are in agreement with the asymptotic theory. A more detailed comparison between theory and experiments is presented in the following text. The radius of curvature of the waves is 10.2 m. The wave crest is intended to hit initially in the middle of the beam. However an air pocket is likely to be created initially.

The rigid body drop velocity of the plate $V(t)$ is shown in figure 5 as a function of time. Three-dimensional flow effects cause a difference in the added mass between the
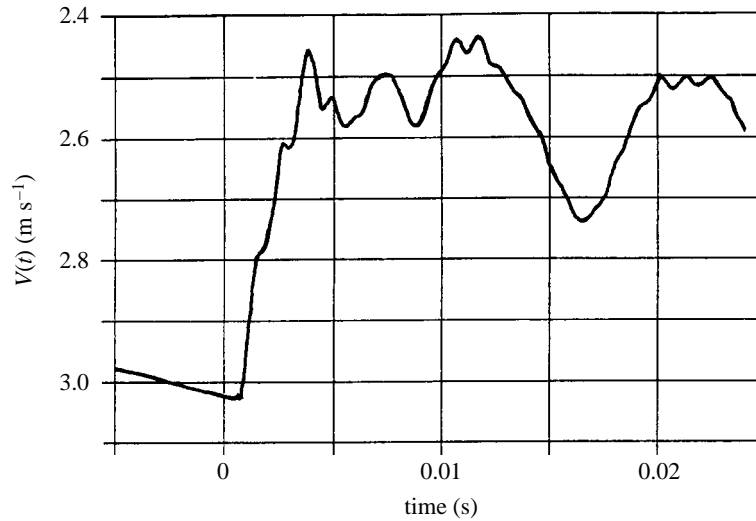
Figure 5. The rigid body velocity of the plate as a function of time. Drop height is 0.5 m.
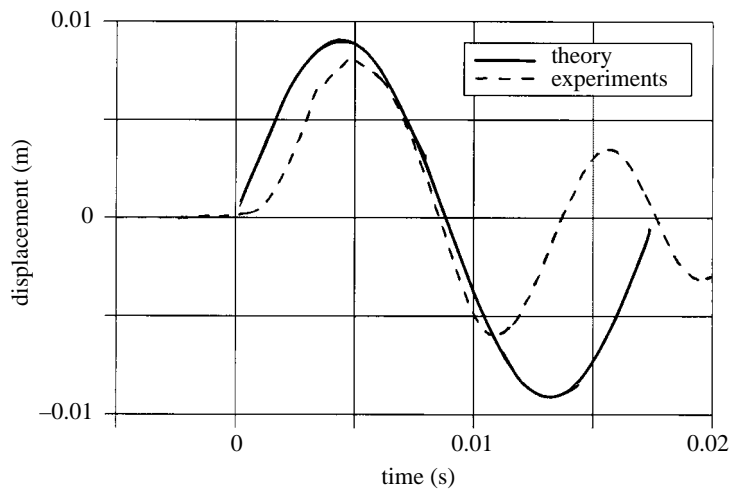

Figure 6. The vertical deflection in the middle of the elastic plate as a function of time. Drop height is 0.5 m.

theory and the model tests. Separate numerical calculations for a rigid flat plate show that the result for the two-dimensional added mass should be reduced by 14%. This reduction implies that the first wet natural period is 6% lower than predicted by a two-dimensional hydrodynamic theory. Since deflections and strains are proportional to the natural period, this implies 6% lower deflection and stress values due to three-dimensional hydrodynamic effects.

Figure 6 shows experimental and theoretical values for the vertical deflection midways between the beam ends as a function of the time. A drop velocity of $2.5 \mathrm{~m~s^{-1}}$ is used in the theoretical results. This is based on examining $V(t)$ and using a representative value after the structural inertia phase. This drop velocity is also used in subsequent figures. Figure 6 shows that initially, the beam deflection is equal to zero and increases to its maximum value after 4–5 ms. The theoretical oscillation period is approximately 17 ms. There is good agreement between the experimental

and numerical values for the maximum deflection and the oscillation period during the first half oscillation period. Accounting for a possible 6% reduction in theoretical values due to three-dimensional flow effects brings the amplitude down from 0.0091 m to 0.0086 m and even closer to experimental values. However, there is a significant difference between theoretical and the experimental values for the deflection and the oscillation period during the second half oscillation period. Since the oscillation period is significantly reduced, this effect cannot be explained by damping. The difference can be explained by the occurrence of cavitation and ventilation in the tests. Figure 7 shows the time history of the measured and theoretical pressures at two positions at the plate. P1 and P3 represent the pressure in the centre of the plate and at a position 100 mm from the centre. The theoretical pressures are obtained using equation (4.17) for $U = 0$. The figure shows that large underpressures relative to atmospheric pressure are present in the second half of the oscillation period. The pressures at P1 and P3 are close to that vapour pressure around time equal to 0.01 s both in theory and experiments. This means cavitation may occur. Due to the large underpressures under the plate during the second half of the first complete oscillation and the low submergence of the plate, air will be drawn in under the plate and the pressure becomes close to atmospheric (see time larger than 0.015 s in figure 7). This means ventilation. This effect is also evident in the measurements of the wetted length, which shows a significant reduction during this time interval. The consequence of this reduction in the wetted length due to ventilation and cavitation is a pronounced reduction in the added mass and hence a reduction in the oscillation period. This causes a lower amplitude. Actually, the oscillation period for time larger than about 0.014 s comes very close to the highest natural period in air. These effects are not included in the theory. However, the maximum deflection and stresses occur during the first half oscillation period and are the most important results from a practical design point of view. The numerical and experimental values are in good agreement for this part of the impact. When it comes to pressures, pronounced peaks are present in the experimental results in the initial phase. These are what often is measured only and referred to as wetdeck slamming pressures. The asymptotic theory in the free vibration phase does not include such effects. The pressures are only associated with 'added mass' effects due to the vibrating beam. By disregarding the experimental peaks in figure 7, there is reasonable agreement between theory and experiments up to cavitation occurs around time equal to 0.01 s.

Figure 8 shows the strains at different locations along the beam as a function of time. In transforming the strains to stresses, 1000 microstrains correspond to a stress level of 210 N mm^{-2}. The agreement between theory and the drop tests is good for the different measurement points along the plate during the first half oscillation period. Similarly as for the deflection, the magnitude of the response and the oscillation period are reduced during the second half period of oscillation. What this implicitly means is that the pressure peaks do not matter for predictions of maximum strains. Kvålsvold *et al.* (1995) presented the measured peak pressures from all the different drop tests as a function of drop speed for different curvatures of the waves and impact positions. There was a tremendous scatter in the pressures at a given drop speed. The maximum reported pressure was close to 80 bar for a drop speed around 6 m s^{-1}. The measured peak pressure results do not encourage the designer to treat the impact problem in a deterministic way even in deterministic environmental conditions. This study indicates that wetdeck slamming may be treated deterministically
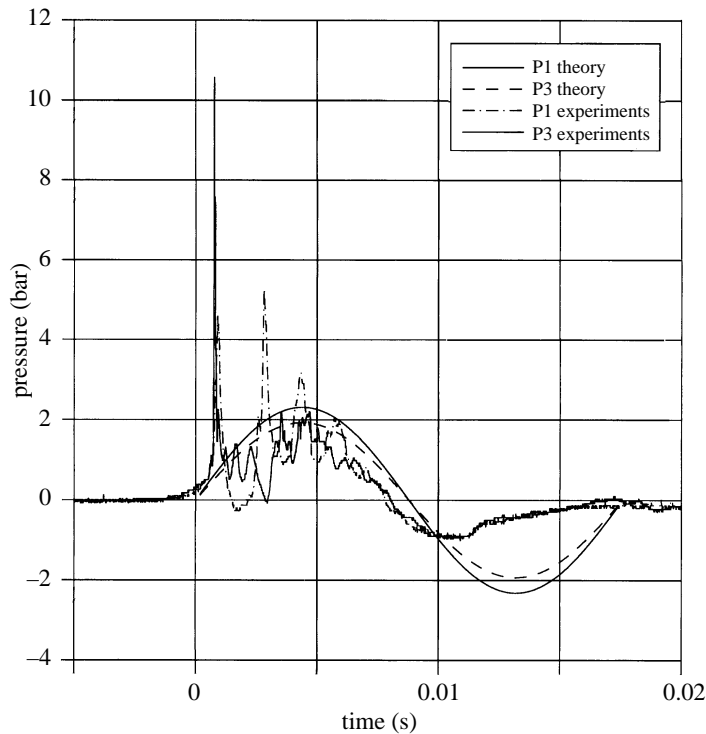
Figure 7. Pressure at two positions of the plate as a function of time, (see figure 4). Comparison between asymptotic theory and drop tests. Drop height is 0.5 m.
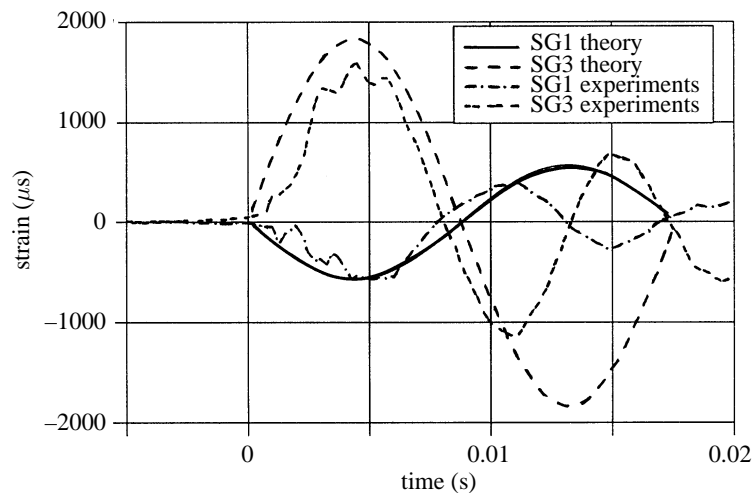

Figure 8. The strains at different locations along the beam as a function of the time, (see figure 4). Comparison between asymptotic theory and drop tests. Drop height is 0.5 m.

in deterministic environmental conditions as long as no attention is paid to the peak pressure.

Kvålsvold *et al.* (1995) also included comparisons with the method by Kvålsvold & Faltinsen (1995). No comparisons were made for pressures. The numerical results were quite similar to what is predicted by the present asymptotic method. A differ-

ence exists for the bending stress where the presence of the second symmetric wet mode was evident. Similar results can be predicted by the asymptotic method by including higher wet modes. The amplitude of the second symmetric wet mode is clearly lower than the amplitude of the first wet mode. However, the experiments do not show a comparable amplitude for the second symmetric wet mode. This can partly be explained by that a measured structural damping of 5% of critical damping for the second symmetric mode was not included in the numerical model. An additional reason may be improper flow description during the initial phases of the flow so that the amplitude of the second symmetric wet mode is initially overpredicted.

6. Conclusions

Wetdeck slamming is studied theoretically by a hydroelastic beam model. Aluminium or steel have implicitly been assumed as a material. The problem is significantly simplified by introducing an initial structural inertia phase and a subsequent free vibration phase. The theoretical development has been inspired by the more complex theory presented by Kvålsvold (1994) and Kvålsvold & Faltinsen (1995). The effect of forward speed is studied theoretically. When the forward speed is large relative to the drop velocity, the problem becomes similar to an unsteady hydrofoil problem in infinite fluid. The results indicate that the effect of the forward speed from the free surface conditions is not important for realistic wetdeck slamming conditions. The important effect comes from the body boundary conditions as an 'angle of attack' effect.

The theoretical model has been compared with drop tests of elastic plates on waves of different steepnesses. No forward speed is included. High pressures occur during the initial phase of the impact. The experimental results suggest that the maximum impact pressures cannot be treated deterministically even in deterministic environmental conditions. The theory does not predict these pressures in a quantitative way. The good agreement between theoretical and experimental bending stresses and deflections shows that it is unnecessary to quantitatively predict the large pressures.

Both the theory and the experiments show that the maximum bending stress is proportional to the drop velocity and is not sensitive to where the waves hit the wetdeck nor to the curvature of the wave crest in the impact region.

The problem is truly hydroelastic in nature. The maximum stresses occur approximately after one fourth of the highest wet natural period. The pressures become negative relative to atmospheric pressure during the second half of the first wet natural oscillation period. This can cause cavitation and ventilation to occur. The theory predicts cavitation to occur at the same time as the experiments. When ventilation has occurred, the plate oscillates like in air.

This study suggests a simple way of stochastically describing wetdeck slamming in an irregular sea. The maximum bending stresses are found to be proportional to the effective local drop velocity V_e given by equation (2.7). This implies that the statistical properties of the bending stresses are described by the stochastic nature of V_e. If the global wave induced motions of the vessel can be described by linear theory, this is standard practice.

References

Aarsnes, J. V. 1994 An experimental investigation of the effect of structural elasticity on slamming loads and structural response. Technical Report, MARINTEK A/S, Trondheim, Norway.

Bisplinghoff, R. L., Ashley, H. & Halfman, R. L. 1955 *Aeroelasticity.* Reading, MA: Addison–Wesley.

Kvålsvold, J. 1994 Hydroelastic modelling of wetdeck slamming on multihull vessels. Ph.D. thesis, Department of Marine Hydrodynamics, The Norwegian Institute of Technology, Norway, MTA-Report 1994:100.

Kvålsvold, J. & Faltinsen, O. 1995 Hydroelastic modelling of wet deck slamming on multihull vessels. *J. Ship Res.* **39**, 225–229.

Kvålsvold, J., Faltinsen, O. & Aarsnes, J. V. 1995 Effect of structural elasticity on slamming against wetdecks of multihull vessels. In *Proc. 6th Int. Symp. on the Practical Design of Ships and Offshore Mobile Units (PRADS), Seoul, South Korea*, pp. 1684–1699.

Miyamoto, T. & Tanizawa, K. 1985 A study of the impact on ship bow (2nd Report). *J. Soc. Naval Arch. Japan* **158**, 270–279.

Ulstein, T. & Faltinsen, O. 1994 Hydroelastic analysis of a flexible bag-structure. *20th Symposium on Naval Hydrodynamics, University of California, Santa Barbara, USA.*

Verhagen, J. H. G. 1967 The impact of a flat plate on a water surface. *J. Ship Research* **11**, 211–223.

Wagner, H. 1932 Über stoss und gleitvergänge an der oberfläche von flössigkeiten. *Z. Ang. Math. Mech.* **12**, 192–253.

Watson, G. N. 1958 *A treatise on the theory of Bessel functions*, 2nd edn. Cambridge University Press.